Inorganic Chemistry

Article

pubs.acs.org/IC

Aluminum-1,4-cyclohexanedicarboxylates: High-Throughput and Temperature-Dependent in Situ EDXRD Studies

Felicitas Niekiel,[†] Maximilian Ackermann,[†] Paul Guerrier,[†] André Rothkirch,[‡] and Norbert Stock*[,†]

[†]Institut für Anorganische Chemie, Christian-Albrechts-Universität zu Kiel, Max-Eyth Straße 2, 24118 Kiel, Germany

[‡]Photon Science, DESY, Notkestraße 85, 22607 Hamburg, Germany

Supporting Information

ABSTRACT: The system $AlCl_3 \cdot 6H_2O$/*cis*-H_2CDC/*trans*-H_2CDC/solvent was systematically investigated with high-throughput methods to study the influence of the two 1,4-cyclohexanedicarboxylate isomers (*cis*- and *trans*-H_2CDC) as flexible aliphatic linker molecules on the formation of new crystalline compounds. Using the *cis*-isomer, the layered inorganic–organic hybrid compound [Al(OH)(*cis*-CDC)] (**1**) is formed. The use of *trans*-H_2CDC leads to the microporous MOF [Al(OH)(*trans*-CDC)]·H_2O (**2**) denoted CAU-13. Its framework is related to the well-known MIL-53, which was previously described for trivalent cations and rigid terephthalate linker molecules. The crystal structures of **1** and **2** were derived from powder X-ray diffraction data. Temperature-dependent in situ energy dispersive X-ray diffraction (EDXRD) experiments for the synthesis of **2** were carried out at HASYLAB, DESY, Hamburg. The kinetic analysis, applying the Gualtieri model to the experimental data, revealed Arrhenius activation energies of 76 kJ/mol for both the nucleation and the growth process. These values do not differ much from the activation energies reported for MOFs with aromatic rigid linker molecules.

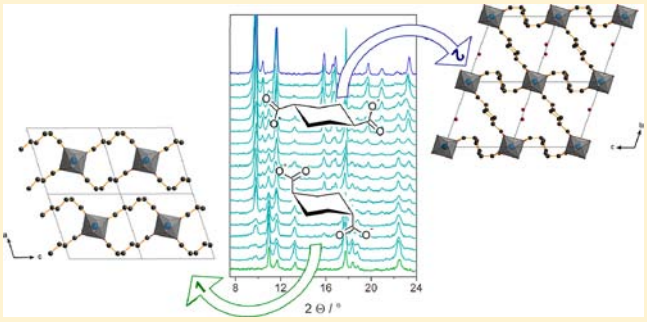

INTRODUCTION

In the class of inorganic–organic hybrid materials, metal–organic frameworks (MOFs) play an extraordinary role as potential materials for gas storage or separation, as catalysts and even drug carriers. This is due to their porosity and modular structure, which allows for tuning of their properties. Most known MOFs contain rigid aromatic di-,[1−3] tri-,[4−6] and tetracarboxylate[7−9] linker molecules, while MOFs built up from flexible linker molecules are still rare: V-shaped linkers bearing an oxo-,[10−12] sulfonyl-,[10] or amine[11,13] bridge between two aromatics allow for a rotation between the aromatic rings. A larger aliphatic bridge results in even more flexible linkers.[14,15]

Aluminum-based MOFs are not only light-weighted and said to be nontoxic but have also proven to be stable against hydrolysis. Unfortunately, Al-based MOFs most often can only be obtained as microcrystalline powders. The structure determination of these compounds is challenging and often requires the combination of different computational tools.[16−20] MOFs are usually synthesized under solvothermal reaction conditions. By employing high-throughput (HT) methods, which make use of the parallelization, miniaturization, and automation of the synthesis and characterization steps,[18,21,22] large parts of the parameter fields can be systematically investigated to discover new compounds. Reaction conditions for a known substance can also be optimized in an admissible amount of time, or systematic investigation of the crystallization fields of certain products can be carried out. Although this method permits establishing reaction trends in the reaction system, no information can be obtained on the crystallization process itself. Hence, in addition to HT experiments, in situ studies[23,24] need to be carried out to get a deeper understanding of the reaction processes during the crystallization. Methods like in situ light scattering,[25,26] in situ EXAFS,[27] in situ AFM,[28] and in situ energy dispersive X-ray diffraction (EDXRD)[24,29,30] are valuable tools to gain insight into the crystallization processes and offer the opportunity for kinetic analyses. In situ EDXRD experiments are usually carried out applying synchrotron radiation. Advantages of synchrotron radiation are the available flux in combination with the energy range used, which allow for penetrating conventional reaction vessels and obtaining data with decent time resolution (<60 s). Thus, the crystallization process can be observed under the same conditions as applied in the laboratory without imposing the reaction to an additional external influence.[31,32] Another advantage of in situ XRD investigations is the observation of potentially occurring crystalline intermediates. For example, in previous in situ EDXRD experiments, the crystalline intermediate MOF-235 could be observed in the crystallization of MIL-53(Fe)[29] and MIL-101-NH_2(Al).[33] The degradation of MOF-14(Cu) to Cu_2O at long reaction times was observed,[30] and kinetic studies on different MOFs applying either conventional electric (CE) or microwave assisted (MW)

Received: April 10, 2013
Published: July 17, 2013

   dx.doi.org/10.1021/ic400825b | *Inorg. Chem.* 2013, 52, 8699−8705

heating were accomplished.[23,24,34] Furthermore reaction mechanisms for the formation of nonporous inorganic−organic hybrid compounds could be postulated,[35,36] and their pH-induced phase transition was observed.[37]

We are interested in the discovery of new aluminum MOFs. Here, we present the results of our investigation using the flexible aliphatic linker molecule 1,4-cyclohexanedicarboxylic acid (H_2CDC) in the system $AlCl_3·6H_2O$/*cis*-H_2CDC/*trans*-H_2CDC/solvent. Applying HT methods, the two new compounds [Al(OH)(*cis*-CDC)] (**1**) and [Al(OH)(*trans*-CDC)]·H_2O (**2**) were discovered, and their reaction conditions were optimized. Both compounds were characterized in terms of thermal stability and sorption behavior. Additionally, the crystallization of **2** was investigated with in situ EDXRD measurements, which allowed us to extract the kinetic parameters.

EXPERIMENTAL SECTION

All reagents and solvents were purchased from commercial sources and used without further purification. Syntheses were carried out under solvothermal conditions in custom-made HT autoclaves with PTFE inserts.[21,38] The in situ EDXRD measurements were carried out at beamline F3 at HASYLAB, DESY, Hamburg using DURAN culture tubes as reactors. X-ray powder diffraction (XRPD) measurements were carried out on a Stoe Stadi P diffractometer in transmission geometry with Cu Kα_1 radiation, equipped with an image plate detector system for the HT-measurements or a linear PSD detector system for high-resolution data. MIR spectra were recorded on a Bruker ALPHA-P FT-IR spectrometer in the spectral range 4000−400 cm^{-1}. For the thermogravimetric analyses under air, a NETSCH STA 409 CD analyzer was used with a heating rate of 4 K/min and an air flow rate of 75 mL/min. N_2 sorption isotherms were recorded at 77 K with a BELSORP-max apparatus (BEL JAPAN INC.). Apparent specific surface areas were calculated using the BET method as described in the literature.[39] Micropore volumes were calculated from the adsorption branch at p/p_0 = 0.5. The high-resolution XRPD pattern for the structure refinement of **2** was measured at beamline P08 at PETRA III, DESY, Hamburg. SEM images were obtained with a Zeiss Ultra55Plus microscope.

HT Experiments. The system $AlCl_3·6H_2O$/*cis*-H_2CDC/*trans*-H_2CDC/solvent was investigated under solvothermal reaction conditions applying our custom-made HT reactors containing 24 PTFE reaction vessels with a maximum volume of 2.0 mL.[38] The solid starting materials (H_2CDC and $AlCl_3·6H_2O$) were placed in the PTFE vessels. Afterward, the solvents (water, DMF, or base) were added, beginning with the addition of water. The combined amount of *cis*- and *trans*-H_2CDC was kept constant at 25 mg (0.15 mmol). The molar ratio of *cis*-:*trans*-H_2CDC was varied stepwise from 0 to 100%, and 35 mg (0.15 mmol) of $AlCl_3·6H_2O$ and a total solvent volume of 500 μL were used. For the synthesis optimization, the concentrations of reactants and/or the solvents were varied. Different bases were applied as additives. The reactor was heated in an oven at 130 °C for 12 h. Product discovery was performed via filtration. The product was dried in air at 75 °C. All reactions are listed in the Supporting Information (Table S2).

Optimized Reaction Conditions for Compound 1. A mixture of 25 mg (0.15 mmol) of *cis*-H_2CDC, 35 mg (0.15 mmol) of $AlCl_3·6H_2O$, 200 μL of H_2O, and 300 μL of 0.1 mM pyridine (in water) was used in the synthesis procedure described above. The crude product was washed with a mixture of ethanol and DMF (80%: 20%) via stirring at ambient temperature for 10 h. Because of the small reaction volume, the yield was not determined. The purity was confirmed by elemental analyses. Anal. Calcd for [Al(OH)(*cis*-CDC)]: C, 44.9; H, 5.18. Found: C, 45.3; H, 5.28. IR spectra are presented in the Supporting Information.

Optimized Reaction Conditions for Compound 2. A mixture of 32 mg (0.19 mmol) of *trans*-H_2CDC, 36 mg (0.15 mmol) of $AlCl_3·6H_2O$, 100 μL of H_2O, and 400 μL of DMF was used in the synthesis procedure described above. Subsequently, the crude reaction product was treated solvothermally (130 °C, 10 h) with DMF, followed by ethanol.

Scale-Up Synthesis of Compound 2. Larger amounts of **2** were synthesized using 37 mL PTFE lined steel autoclaves applying a reaction volume of 20 mL. A mixture of 516 mg (3.00 mmol) of *trans*-H_2CDC and 724 mg (3.00 mmol) of $AlCl_3·6H_2O$ was placed in the PTFE vessel, and 16.0 mL of DMF and 4.00 mL of H_2O were added. The reactor was heated in an oven at 130 °C for 12 h. For the scaled-up synthesis employing MW-assisted heating, the same amounts of starting materials were mixed in a microwave tube (Biotage, 5−20 mL glass reactor), which was sealed with a septum. The reaction mixture was heated in a microwave oven (Biotage Injector) for 45 min at 130 °C under stirring. Purification was also performed via MW-assisted heating (130 °C, 45 min each step). The purity was confirmed by elemental analyses. Anal. Calcd for [Al(OH)(*trans*-CDC)]·1.5H_2O: C, 39.8; H, 5.85. Found: C, 36.7; H, 5.55. IR spectra are presented in the Supporting Information. Yield (CE heating), 495 mg (71%); yield (MW heating), 440 mg (63%).

Activation of 1 and 2. Before the N_2 sorption experiments, the washed compounds were thermally activated. Compound **1** was heated for 3 h at 150 °C in a vacuum ($p \leq 10^{-2}$ kPa); compound **2** was heated for 12 h at 200 °C in a vacuum ($p \leq 10^{-2}$ kPa).

In Situ Crystallization Experiments. The temperature-dependent EDXRD experiments were carried out at beamline F3, HASYLAB at DESY, Hamburg, Germany. Reactions were performed in Schott Duran glass culture tubes, which were heated in a custom-made reactor system with an external thermostat.[40,41] The scattered white beam synchrotron radiation (4−55 keV) was detected by a liquid nitrogen cooled germanium semiconductor detector system. The detector angle was set to 2.2°. The collimator slits were set to 0.2 × 0.2 mm^2. The starting materials (105 mg (0.61 mmol) of *trans*-H_2CDC, 121 mg (0.50 mmol) of $AlCl_3·6H_2O$, 400 μL of H_2O, and 1600 μL of DMF) were homogenized in the Duran tube by shaking. The reaction mixture was transferred to the preheated vessel in the in situ reactor system. The reactions were carried out under stirring at 105, 110, 115, 120, and 130 °C.

Structure Determination. All crystal data and the results of the structure refinement of compound **1** and **2** are summarized in Table 1. Bond lengths are given in the Supporting Information (Tables S4 and S5).

Crystal Structure Determination of [Al(OH)(*cis*-CDC)] (1). The structural model of **1** was obtained from the isostructural compound [Fe(OH)(*cis*-CDC)],[42] and the structure was refined from laboratory X-ray powder diffraction data (Cu Kα_1 radiation). The powder pattern was successfully indexed using TOPAS-Academic[44] (a = 8.033(2), b = 6.648(2), c = 8.523(2) Å, α = 90°, β = 108.339(2)°, γ = 90°). Comparing the lattice parameters with the ones reported for [Fe(OH)(*cis*-CDC)],[42] it can be seen that they are very similar (a = 8.010(2), b = 6.8872(18), c = 8.569(2) Å, α = 90°, β = 108.232(5)°, γ = 90°), so this structure was directly used as a starting model. After replacement of Fe^{3+} by Al^{3+} ions, the model was refined by the Rietveld technique using TOPAS-Academic 4.1.[44] A Thompson−Cox−Hastings profile function and a simple axial model were used for profile fitting. Preferred orientation was modeled using a fourth-order spherical harmonics series. Soft distance restrains were applied on the C−C bond between the carboxylate and the neighboring carbon atom (C1−C2).

Crystal Structure Determination of [Al(OH)(*trans*-CDC)]·H_2O (2). The crystal structure of **2** was determined from powder X-ray diffraction data obtained at beamline P08, PETRA III at DESY, Hamburg. The sample was measured in a 0.5 mm quartz capillary at a wavelength of λ = 0.825986 Å. For the experimental setup of the beamline, see ref 45. The powder pattern was indexed, and the cell parameters were refined using TOPAS-Academic[44] (a = 6.6156(5), b = 9.4322(8), and c = 9.4657(9) Å, α = 107.581(5)°, β = 107.714(11)°, γ = 93.198(5)°). The structure was solved in the space group $P\bar{1}$ by direct methods using the program EXPO 2009.[43] The positions of all framework atoms were visible from the structure solution in EXPO 2009. The extracted atomic positions were set as the structural starting

dx.doi.org/10.1021/ic400825b | Inorg. Chem. 2013, 52, 8699−8705

Table 1. Summary of the Crystallographic Parameters of the Structure Refinement of 1 and 2

	[Al(OH)(*cis*-CDC)] (**1**)	[Al(OH)(*trans*-CDC)]·H_2O (**2**)
structure determined from	powder data	powder data
λ/Å	1.5406	0.825986
formula sum	$AlC_8H_{11}O_5$	$AlC_8H_{13}O_6$
Z	2	2
crystal system	monoclinic	triclinic
a/Å	8.0265(2)	6.6169(5)
b/Å	6.6425(1)	9.4300(6)
c/Å	8.5155(2)	9.4642(6)
α/deg	90	107.577(3)
β/deg	108.329(2)	107.725(7)
γ/deg	90	93.209(5)
V/Å^3	430.99(2)	529.08(7)
space group	$P2_1/m$	$P\bar{1}$
solution method	structural model from the literature[42]	direct methods, Expo2009[43]
refinement method	least-squares Rietveld method[44]	least-squares Rietveld method[44]
R_{wp}	8.79	5.33
R_{Bragg}	3.24	1.70
GOF	1.53	1.87

model for the Rietveld refinement with TOPAS-Academic. A Split Pearson VII profile function and a simple axial model were used for profile fitting. Preferred orientation was modeled using a fourth-order spherical harmonics series. Soft distance and angle restrains were applied to the C−C and C−O bonds of the organic linker molecule. From the difference Fourier map, the position of one additional water molecule per formula unit located inside the channels of the framework was extracted.

RESULTS AND DISCUSSION

HT Experiments. The HT investigation of the system $AlCl_3·6H_2O$/*cis*-H_2CDC/*trans*-H_2CDC/solvent resulted in the discovery of the two new phases [Al(OH)(*cis*-CDC)] (**1**) and [Al(OH)(*trans*-CDC)]·H_2O (**2**). Both compounds crystallize from a mixture of water and DMF (volume ratio = 2:3) at a reaction temperature of 130 °C. The XRPD patterns of the products obtained when varying the reactant ratios *trans*-H_2CDC:*cis*-H_2CDC from 0% to 100% are presented in Figure 1. Only when applying 100% of *cis*- or *trans*-H_2CDC can the respective phases **1** or **2** be obtained phase-pure.

Because the crystallinity of compound **1** was not sufficiently good to carry out the structure determination, the reaction conditions had to be optimized. These studies resulted in drastically changed reaction conditions. The addition of DMF either in the reaction mixture or during solvothermal purification led to a decrease of the crystallinity of the product. Because the addition of bases has proven to increase the crystallinity of MOFs,[17] different bases were used in the reaction mixture for the synthesis of **1**. The best results were obtained using highly diluted aqueous pyridine as additive. The XRPD patterns of the different products starting from product discovery up to the optimized reaction conditions are presented in Figure S1.

Structure Description of [Al(OH)(*cis*-CDC)] (1). **1** is isostructural to [Fe(OH)(*cis*-CDC)].[42] The structure of **1** was refined from powder diffraction data obtained from a laboratory X-ray source. The final Rietveld plot is given in Figure 2 (top). Zigzag chains of *trans*-corner sharing AlO_6-octahedra are

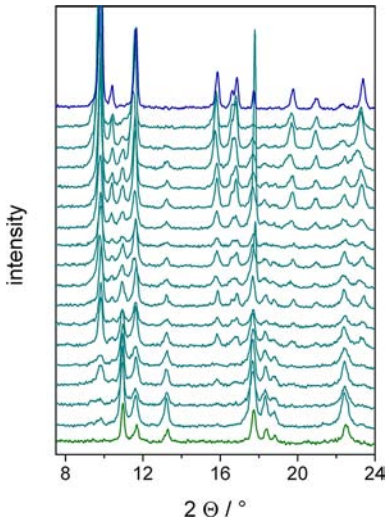

Figure 1. XRPD pattern series of the reaction products obtained from the HT experiment in the system $AlCl_3·6H_2O$/*cis*-H_2CDC/*trans*-H_2CDC/solvent with an increasing ratio *trans*-H_2CDC:*cis*-H_2CDC (from bottom to top: 0%, 5%, 10%, 20%, 25%, 30%, 40%, 45%, 50%, 55%, 60%, 65%, 70%, 75%, 80%, 90%, 95%, and 100% of *trans*-H_2CDC); green, **1**; dark cyan, mixtures of **1** and **2**; blue, **2**.

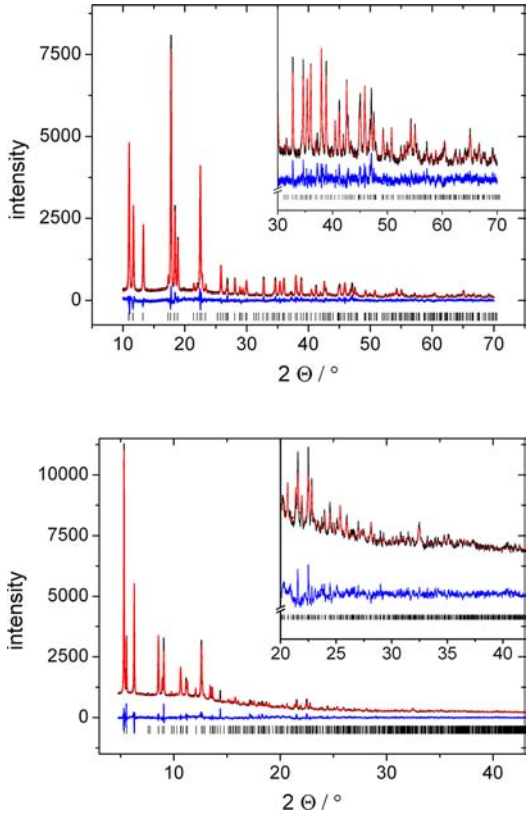

Figure 2. Final Rietveld plot of the structure refinement of **1** (top, λ = 1.5406 Å) and **2** (bottom, λ = 0.825986 Å). The observed powder patterns are shown in black, the calculated powder patterns as an overlay are in red, and the difference plots (observed-calculated) are in blue. The tics mark the allowed Bragg peak positions.

connected to each other via *cis*-CDC^{2-} linkers to layers in the *b*,*c*-plane. The layers are connected along the *a*-axis by van-der-Waals interactions (Figure 3). The asymmetric unit and a

dx.doi.org/10.1021/ic400825b | Inorg. Chem. 2013, 52, 8699−8705

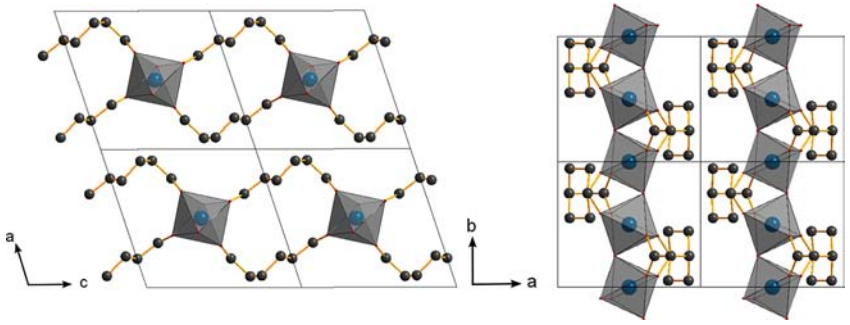

Figure 3. Structure of **1** viewed along the *b*-axis (left) and the *c*-axis (right). AlO_6 polyhedra are represented as gray octahedra. Carbon atoms are shown as black spheres.

table of the bond lengths are presented in the Supporting Information (Figure S5 and Table S4, respectively).

Structure Description of [Al(OH)(*trans*-CDC)]·H_2O (2). The structure of **2** was solved and refined from powder X-ray diffraction data obtained at the synchrotron beamline P08, PETRA III at DESY, Hamburg with a wavelength of λ = 0.825986 Å. The final Rietveld plot is given in Figure 2 (bottom). The framework structure is built up from two crystallographically independent CDC^{2-} and Al^{3+} ions. The latter are octahedrally surrounded by six oxygen atoms. Four of these belong to the carboxylate groups of the CDC^{2-} ions (O2, O3 and O4, O5, respectively). The oxygen atom O1 belongs to a μ-OH-group connecting the AlO_6-octahedra to form *trans* corner sharing zigzag chains along the *a*-axis. This structural motif is well-known from the MIL-53 family.[46−48] Each chain is connected to four other chains via *trans*-CDC^{2-} ions resulting in rhombohedrically shaped one-dimensional pores (Figure 4).

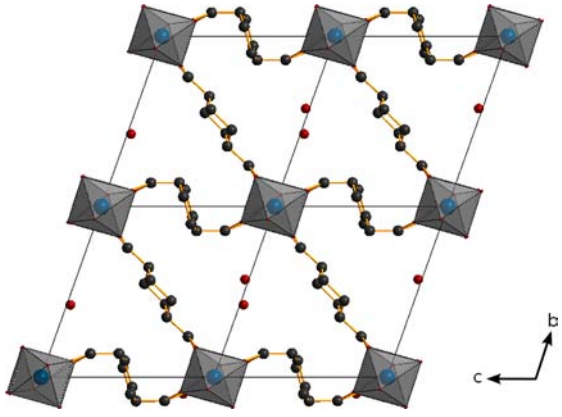

Figure 4. Crystal structure of **2**. View along the *a*-axis. AlO_6 polyhedra are represented by gray octahedra. Oxygen atoms of the water molecules are shown as red, and carbon atoms are shown as black spheres.

Like in the isostructural In-compound, the cyclohexane ring is either in the *e,e*- or in the *a,a*-conformation (Figure 5 and Figure S6).[49] While in the solid starting material only the *e,e*-conformer is present,[50] equilibration upon dissolution leads to a mixture of the *e,e*- and the *a,a*-conformer, which are subsequently incorporated in the structure of **2**. Inside the pores, two water molecules (OW) per unit cell are located. The asymmetric unit and the bond lengths are given in Figure S6 and Table S5.

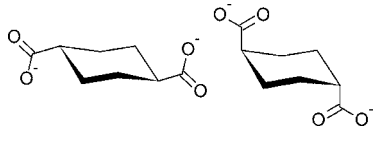

Figure 5. Both conformers of *trans*-CDC^{2-} observed as part of the framework of **2**: *e,e*-conformation (left) and *a,a*-conformation (right).

Thermogravimetric Analysis. The thermal stability of the compounds was investigated by thermogravimetric analyses (4 K/min, air flow). In the TG curve of **1**, a one-step weight loss beginning at a temperature of ~350 °C is observed. This loss of 79% corresponds to the decomposition of the compound yielding Al_2O_3 (calculated: −76%). Compound **2** shows a two-step weight loss. The first step up to 100 °C corresponds to a removal of water molecules (experimental, −11%; calculated for [Al(OH)(*trans*-CDC)]·1.25H_2O, −9.5%). A plateau in the TG curve up to 350 °C can be observed. The next weight loss of 70% stems from the decomposition of the framework (calculated: −69%). The different numbers of adsorbed water molecules determined from elemental and TG analyses stem from the different experimental setup. Both TG curves are presented in the Supporting Information (Figures S7 and S8, respectively).

Sorption Experiments. Nitrogen sorption experiments were performed at 77 K. Before the experiments, the as-synthesized products were purified and activated to remove unreacted starting materials and/or solvent molecules. Solvent exchange was performed as described in the Experimental Section. When **1** is treated solvothermally with DMF, a remarkable loss of crystallinity was observed (Figure S3), so different routes for the purification of the compounds had to be found. Therefore, **1** was stirred in an ethanol/DMF mixture at ambient conditions overnight. Compound **2** was first treated solvothermally with DMF to remove unreacted *trans*-H_2CDC and then with ethanol to remove the DMF from the pores. The conditions of the subsequent thermal activation and results of the BET analysis are given in Table 2, and the sorption isotherms are presented in Figure 6.

Because of the layered structure, compound **1** does not exhibit any porosity toward N_2. Compound **2** shows a type I isotherm typical for microporous materials.[51]

In Situ Crystallization Experiments. Temperature-dependent in situ crystallization experiments were performed for compound **2**. In situ EDXRD measurements allow a direct observation of the crystallization process in the reaction vessel. Reactions were performed at five different temperatures between 105 and 130 °C. The extent of crystallization $\alpha(t) = I(t)/I(t_\infty)$ was determined by normalization of the integral of

dx.doi.org/10.1021/ic400825b | Inorg. Chem. 2013, 52, 8699−8705

Table 2. Activation Conditions, Specific Surface Areas, and Micropore Volumes of 1 and 2

	[Al(OH)(*cis*-CDC)] (**1**)	[Al(OH)(*trans*-CDC)] (**2**)
activation temp [°C]	150	200
activation time at $p \leq 10^{-2}$ kPa (h)	3	12
$a_{s,BET}$ [m^2/g]	77	378
$V_{micro,p/p_0 = 0.5}$ [cm^3/g]		0.15

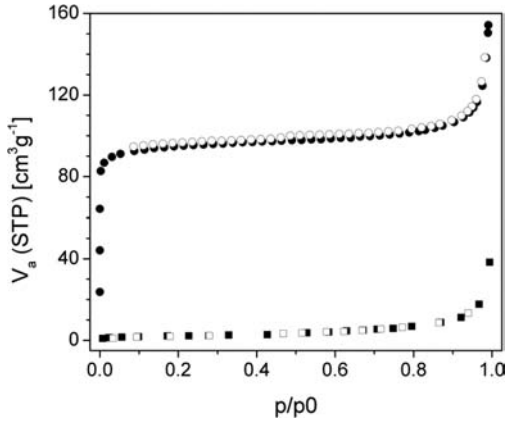

Figure 6. N_2 sorption isotherms for **1** (squares) and **2** (circles). Filled symbols mark the adsorption, while empty symbols mark the desorption branch.

the most intense reflection at time t to the value at the time of complete crystallization (t_∞). Because the signal between 35 and 38 keV is composed of two strongly overlapping peaks (36 keV (d = 9.3 Å) and 37 keV (d = 9.0 Å), respectively, Figure S11), brute force methods were applied for data deconvolution assuming a superposition of two Gaussian functions. After setting boundary conditions for each peak position, peak offset and peak width possible superpositions were tested, and the best match to the data was automatically determined.

In Figure 7, the EDXRD patterns for the crystallization at T = 115 °C are presented. At this temperature, the formation of a

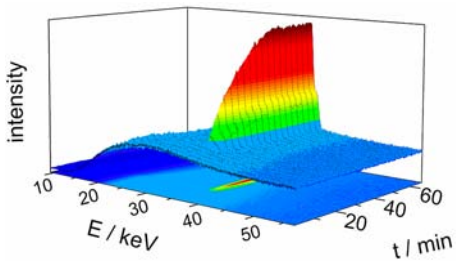

Figure 7. EDXRD patterns of the crystallization of **2** at 115 °C as a function of time. Combined illustration of a surface (top) and contour plot (bottom).

crystalline product can be observed after an induction time of 17 min. The product was filtered off and identified as **2** by powder X-ray diffraction (Figure S14). A comparison of $\alpha(t)$ for the given temperatures shows a decrease of induction as well as reaction times with increasing temperature (Figure 8).

The kinetic analysis was performed applying the Gualtieri model, which was originally developed to describe zeolite crystallization,[52] but has recently also been applied in the

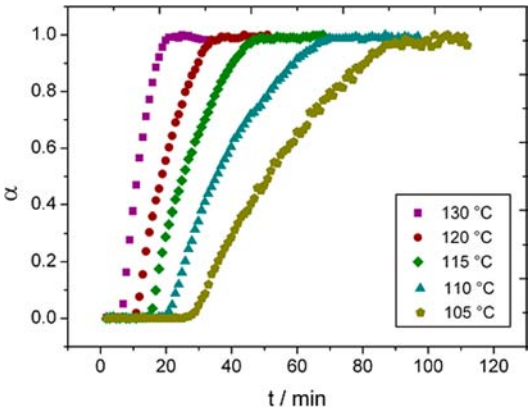

Figure 8. Extent of crystallization of **2** as a function of time derived from the normalized integrals of the most intense reflection observed in the EDXRD patterns.

evaluation of other crystallization processes.[30,34,53−55] In this model, the extent of crystallization is described by:

$$\alpha(t) = \left(\frac{1}{1 + \exp\left(-\frac{t-a}{b}\right)}\right)(1 - \exp(-(k_g t)^n)) \quad (1)$$

The formation of the product is described considering different reaction rates for nucleation (first part of eq 1) and crystal growth k_g. The parameters a and b are constants correlated to the nucleation probability (and thus to the nucleation rate constant $k_n = a^{-1}$), and n is an integer related to the geometry of crystal growth. One-dimensional growth resulting in needle-like crystals would result in a value of n = 1. Simultaneous growth in two dimensions as observed in sheet-like crystallization corresponds to a value of n = 2, and homogeneous growth in all directions is described by a value of n = 3. A first fit to the data resulted in values of $n \approx 2.8$. Thus, homogeneous growth in all dimensions was expected, and n was fixed to 3 before final fitting was performed. The assumption of homogeneous three-dimensional growth was confirmed by SEM images (Figure S12) showing bloc-shaped particles. The constants a and b can be used to express the probability function of nucleation $P_N(t)$ (eq 2).[52]

$$P_N(t) = \exp\left(-\frac{(t-a)^2}{2b^2}\right) \quad (2)$$

In Figure 9, fits of the observed extent of crystallization obtained from integration of the first reflection using the Gualtieri model are given for crystallization at reaction temperatures of 115 and 130 °C, respectively. The plots corresponding to reaction temperatures of 105, 110, and 120 °C and a summary of the kinetic parameters obtained from the fits are given in the Supporting Information (Figure S13 and Table S6, respectively). With the exception of small deviations at the beginning of the crystallization, which is due to the small intensity of the peak in combination with a small signal-to-noise ratio, the model agrees well with the experiments. The probability function of nucleation (eq 2) turns out to be broader for lower reaction temperatures (Figure 9). From the extracted reaction rates, an Arrhenius plot (Figure 10) was prepared.

Activation energies of $E_{A,n}$ = 77 kJ/mol and $E_{A,g}$ = 76 kJ/mol as well as pre-exponential factors of $A_n = 7.9 \times 10^8$ min^{-1} and

dx.doi.org/10.1021/ic400825b | Inorg. Chem. 2013, 52, 8699−8705

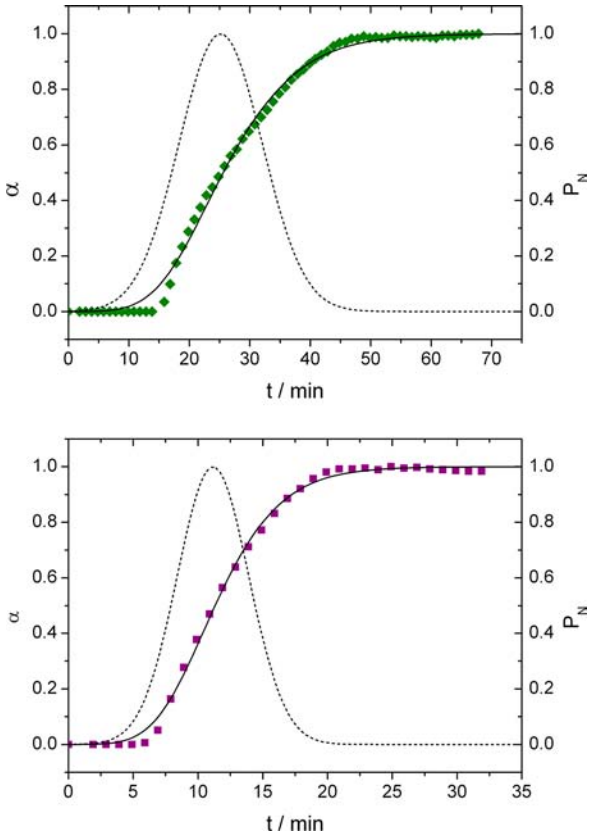

Figure 9. Gualtieri fits of the reactions at temperatures of 115 (top) and 130 °C (bottom). Straight lines represent the fitting function, while dashed lines are the probability function P_N of nucleation. Experiment data are denoted by symbols.

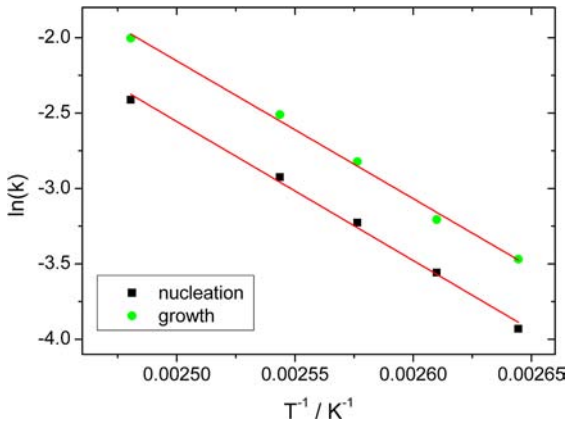

Figure 10. Arrhenius plots for the nucleation (■) and crystal growth (●) of compound **2**. Red lines represent linear fits to the data.

$A_g = 9.6 \times 10^8$ min^{-1} were determined for nucleation and growth processes, respectively. The activation energies are in the range of values observed for the crystallization of Al-MOFs, which are 136 kJ/mol (CAU-1-$(OH)_2$)[24] and 82 and 94 kJ/mol (MIL-101-NH_2(Al))[33] for nucleation and growth, respectively. Typical Arrhenius activation energies for Cu- and Mn-MOFs derived applying the Gualtieri model are in the same range ($E_{A,n}$ = 72−127 kJ/mol and $E_{A,g}$ = 48−99 kJ/mol for HKUST-1,[30] MOF-14,[30] MIL-100(Mn),[56] CPO-27(Ni), and CPO-27(Co)).[34] Thus, the values are in the range observed for MOFs with rigid aromatic linker molecules. In the crystallization of MOFs, different activation energies for nucleation and growth are usually observed.[34] Exeptions are the modulated synthesis of ZIF-8 and the synthesis of CAU-13 described here. For the modulated synthesis of ZIF-8, the pre-exponential factors differ by the factor 10 ($A_n = 2.6 \times 10^7$ min^{-1} and $A_g = 1.3 \times 10^8$ min^{-1}), while the activation energies are very similar ($E_{A,n}$ = 69 kJ/mol and $E_{A,g}$ = 72 kJ/mol).[55] No such differences can be observed regarding the crystallization of CAU-13.

CONCLUSION

Applying HT methods, we were able to investigate the system $AlCl_3 \cdot 6H_2O$/*cis*-H_2CDC/*trans*-H_2CDC/solvent systematically. Two new crystalline phases were found, and their structure was solved (**2**) and refined (**1** and **2**) from X-ray powder diffraction data: [Al(OH)(*cis*-CDC)] (**1**) exhibits a layered structure; the microporous MOF [Al(OH)(*trans*-CDC)]·H_2O, CAU-13 (**2**) is structurally related to the MIL-53 family. It could be shown that under the chosen conditions pure-phase products of **1** and **2** were obtained when pure *trans*- or *cis*-H_2CDC was used. Exploring mixtures of both isomers does not lead to a new "mixed-linker" product, which was easily demonstrated by HT methods. In situ EDXRD measurements were carried out to gain further insight into the formation process of **2**. The kinetic analysis allowed for the extraction of activation energies. It could be shown that the activation energies of **2** are in the range of activation energies obtained for MOFs with rigid linker molecules.

ASSOCIATED CONTENT

Supporting Information

Exact amounts used for the HT syntheses, XRPD patterns, TG curves, IR spectra, images of the asymmetric units, bond length tables, Gualtieri fits of the extent of crystallization, and material corresponding to the in situ analyses. This material is available free of charge via the Internet at http://pubs.acs.org.

AUTHOR INFORMATION

Corresponding Author

*Tel.: +49-431-880-1675. Fax: +49-431-880-1775. E-mail: stock@ac.uni-kiel.de.

Notes

The authors declare no competing financial interest.

ACKNOWLEDGMENTS

We thank the DFG (SPP 1362) for financial support. Portions of this research were carried out at the light sources DORIS III and PETRA III at DESY, a member of the Helmholtz Association (HGF). We thank DESY for beamtime, in particular Dr. Carsten Deiter (DESY) for the assistance at beamline P08 and Prof. Bensch (University of Kiel) and his group for the equipment and the help at beamline F3.

REFERENCES

(1) Eddaoudi, M.; Kim, J.; Rosi, N.; Vodak, D.; Wachter, J.; O'Keeffe, M.; Yaghi, O. M. *Science* **2002**, *295*, 469.
(2) Férey, G.; Mellot-Draznieks, C.; Serre, C.; Millange, F.; Dutour, J.; Surble, S.; Margiolaki, I. *Science* **2005**, *309*, 2040.
(3) Reinsch, H.; Marszalek, B.; Wack, J.; Senker, J.; Gil, B.; Stock, N. *Chem. Commun.* **2012**, *48*, 9486.
(4) Chui, S. S.-Y.; Lo, S. M.-F.; Charmant, J. P. H.; Orpen, A. G.; Williams, I. D. *Science* **1999**, *283*, 1148.

(5) Feyand, M.; Mugnaioli, E.; Vermoortele, F.; Bueken, B.; Dieterich, J. M.; Reimer, T.; Kolb, U.; de Vos, D.; Stock, N. *Angew. Chem., Int. Ed.* **2012**, *51*, 10373.
(6) Reinsch, H.; Krüger, M.; Wack, J.; Senker, J.; Salles, F.; Maurin, G.; Stock, N. *Microporous Mesoporous Mater.* **2012**, *157*, 50.
(7) Moreau, F.; Audebrand, N.; Poriel, C.; Moizan-Basle, V.; Ouvry, J. *J. Mater. Chem.* **2011**, *21*, 18715.
(8) Lin, X.; Telepeni, I.; Blake, A. J.; Dailly, A.; Brown, C. M.; Simmons, J. M.; Zoppi, M.; Walker, G. S.; Thomas, K. M.; Mays, T. J.; Hubberstey, P.; Champness, N. R.; Schröder, M. *J. Am. Chem. Soc.* **2009**, *131*, 2159.
(9) Hu, Y.-X.; Ma, H.-B.; Zheng, B.; Zhang, W.-W.; Xiang, S.; Zhai, L.; Wang, L.-F.; Chen, B.; Ren, X.-M.; Bai, J. *Inorg. Chem.* **2012**, *51*, 7066.
(10) Lin, J.-D.; Long, X.-F.; Lin, P.; Du, S.-W. *Cryst. Growth Des.* **2010**, *10*, 146.
(11) Martin, D. P.; Supkowski, R. M.; LaDuca, R. L. *Inorg. Chem.* **2007**, *46*, 7917.
(12) Pramanik, S.; Zheng, C.; Zhang, X.; Emge, T. J.; Li, J. *J. Am. Chem. Soc.* **2011**, *133*, 4153.
(13) Yang, Q.; Chen, X.; Cui, J.; Hu, J.; Zhang, M.; Qin, L.; Wang, G.; Lu, Q.; Zheng, H. *Cryst. Growth Des.* **2012**, *12*, 4072.
(14) Qian, J.; Yoshikawa, H.; Zhang, J.; Zhao, H.; Awaga, K.; Zhang, C. *Cryst. Growth Des.* **2009**, *9*, 5351.
(15) Lloyd, G. O.; Atwood, J. L.; Barbour, L. J. *Chem. Commun.* **2005**, *0*, 1845.
(16) Feyand, M.; Mugnaioli, E.; Vermoortele, F.; Bueken, B.; Dieterich, J. M.; Reimer, T.; Kolb, U.; de Vos, D.; Stock, N. *Angew. Chem.* **2012**, *124*, 10519.
(17) Reinsch, H.; Feyand, M.; Ahnfeldt, T.; Stock, N. *Dalton Trans.* **2012**, *41*, 4164.
(18) Volkringer, C.; Loiseau, T.; Guillou, N.; Férey, G.; Haouas, M.; Taulelle, F.; Elkaim, E.; S tock, N. *Inorg. Chem.* **2010**, *49*, 9852.
(19) Senkovska, I.; Hoffmann, F.; Fröba, M.; Getzschmann, J.; Böhlmann, W.; Kaskel, S. *Microporous Mesoporous Mater.* **2009**, *122*, 93.
(20) Ahnfeldt, T.; Guillou, N.; Gunzelmann, D.; Margiolaki, I.; Loiseau, T.; Férey, G.; Senker, J.; Stock, N. *Angew. Chem., Int. Ed.* **2009**, *48*, 5163.
(21) Stock, N. *Microporous Mesoporous Mater.* **2010**, *129*, 287.
(22) Biemmi, E.; Christian, S.; Stock, N.; Bein, T. *Microporous Mesoporous Mater.* **2009**, *117*, 111.
(23) Feyand, M.; Näther, C.; Rothkirch, A.; Stock, N. *Inorg. Chem.* **2010**, *49*, 11158.
(24) Ahnfeldt, T.; Moellmer, J.; Guillerm, V.; Staudt, R.; Serre, C.; Stock, N. *Chem.-Eur. J.* **2011**, *17*, 6462.
(25) Cravillon, J.; Nayuk, R.; Springer, S.; Feldhoff, A.; Huber, K.; Wiebcke, M. *Chem. Mater.* **2011**, *23*, 2130.
(26) Hermes, S.; Witte, T.; Hikov, T.; Zacher, D.; Bahnmuller, S.; Langstein, G.; Huber, K.; Fischer, R. *J. Am. Chem. Soc.* **2007**, *129*, 5324.
(27) Surblé, S.; Millange, F.; Serre, C.; Férey, G.; Walton, R. I. *Chem. Commun.* **2006**, 1518.
(28) Shoaee, M.; Anderson, M. W.; Attfield, M. P. *Angew. Chem., Int. Ed.* **2008**, *47*, 8525.
(29) Millange, F.; Medina, M. I.; Guillou, N.; Férey, G.; Golden, K. M.; Walton, R. I. *Angew. Chem., Int. Ed.* **2010**, *49*, 763.
(30) Millange, F.; El Osta, R.; Medina, M. E.; Walton, R. I. *CrystEngComm* **2011**, *13*, 103.
(31) O'Brien, M. G.; Beale, A. M.; Weckhuysen, B. M. *Chem. Soc. Rev.* **2010**, *39*, 4767.
(32) Pienack, N.; Bensch, W. *Angew. Chem.* **2011**, *123*, 2062.
(33) Juan-Alcaniz, J.; Goesten, M.; Martinez-Joaristi, A.; Stavitski, E.; Petukhov, A. V.; Gascon, J.; Kapteijn, F. *Chem. Commun.* **2011**, *47*, 8578.
(34) Walton, R. I., personal communication.
(35) Schmidt, C.; Feyand, M.; Rothkirch, A.; Stock, N. *J. Solid State Chem.* **2012**, *188*, 44.
(36) Feyand, M.; Hübner, A.; Rothkirch, A.; Wragg, D. S.; Stock, N. *Inorg. Chem.* **2012**, *51*, 12540.
(37) Schmidt, C.; Stock, N. *Inorg. Chem.* **2012**, *51*, 3108.
(38) Stock, N.; Bein, T. *Angew. Chem., Int. Ed.* **2004**, *43*, 749.
(39) Rouquerol, J.; Llewellyn, P.; Rouquerol, F.; Rodriquez-Reinoso, F.; Seaton, N. *Studies in Surface Science Catalysis*; Elsevier: New York, 2007; Vol. *160*, p 49.
(40) Engelke, L.; Schaefer, M.; Schur, M.; Bensch, W. *Chem. Mater.* **2001**, *13*, 1383.
(41) Engelke, L.; Schaefer, M.; Porsch, F.; Bensch, W. *Eur. J. Inorg. Chem.* **2003**, *2003*, 506.
(42) Zheng, Y.-Z.; Chen, X.-M. *Dalton Trans.* **2012**, *41*, 11989.
(43) Altomare, A.; Camalli, M.; Cuocci, C.; Giacovazzo, C.; Moliterni, A.; Rizzi, R. *J. Appl. Crystallogr.* **2009**, *42*, 1197.
(44) Coelho, A. A. *TOPAS-Academic, 4.1*; Coelho Software: Brisbane, 2007.
(45) Seeck, O. H.; Deiter, C.; Pflaum, K.; Bertam, F.; Beerlink, A.; Franz, H.; Horbach, J.; Schulte-Schrepping, H.; Murphy, B. M.; Greve, M.; Magnussen, O. *J. Synchrotron Radiat.* **2012**, *19*, 30.
(46) Serre, C.; Millange, F.; Thouvenot, C.; Noguès, M.; Marsolier, G.; Louër, D.; Férey, G. *J. Am. Chem. Soc.* **2002**, *124*, 13519.
(47) Biswas, S.; Ahnfeldt, T.; Stock, N. *Inorg. Chem.* **2011**, *50*, 9518.
(48) Loiseau, T.; Serre, C.; Huguenard, C.; Fink, G.; Taulelle, F.; Henry, M.; Bataille, T.; Férey, G. *Chem.-Eur. J.* **2004**, *10*, 1373.
(49) Wang, L.; Song, T.; Li, C.; Xia, J.; Wang, S.; Wang, L.; Xu, J. *J. Solid State Chem.* **2012**, *190*, 208.
(50) Dunitz, J. D.; Strickler, P. *Helv. Chim. Acta* **1966**, *49*, 2505.
(51) Sing, K. S. W. *Pure Appl. Chem.* **1982**, *54*, 2201.
(52) Gualtieri, A.; Norby, P.; Artioli, G.; Hanson, J. *Phys. Chem. Miner.* **1997**, *24*, 191.
(53) Antonova, E.; Seidlhofer, B.; Wang, J.; Hinz, M.; Bensch, W. *Chem.-Eur. J.* **2012**, *18*, 1 5316.
(54) Seidlhofer, B.; Antonova, E.; Wang, J.; Schinkel, D.; Bensch, W. *Z. Anorg. Allg. Chem.* **2012**, *638*, 2555.
(55) Cravillon, J.; Schroder, C. A.; Bux, H.; Rothkirch, A.; Caro, J.; Wiebcke, M. *CrystEngComm* **2012**, *14*, 492.
(56) Reinsch, H.; Stock, N. *CrystEngComm* **2013**, *15*, 544.